Catal Lett (2016) 146:518–524
DOI 10.1007/s10562-015-1671-8

Ternary CoAgPd Nanoparticles Confined Inside the Pores of MIL-101 as Efficient Catalyst for Dehydrogenation of Formic Acid

Nan Cao[1] · Shiyi Tan[1] · Wei Luo[1,2] · Kai Hu[1] · Gongzhen Cheng[1]

Received: 28 September 2015 / Accepted: 30 November 2015 / Published online: 31 December 2015

Abstract Highly dispersed ternary CoAgPd nanoparticles with different composition have been successfully immobilized on the metal-organic frameworks (MIL-101) by using a simple liquid impregnation method for the first time. The molecular scale electronic synergistic effect between non-noble metal Co and AgPd NPs and the confinement effect of MIL-101 are the crucial roles for the improvement of catalytic performances toward dehydrogenation of formic acid under mild conditions. The resultant catalysts are composition dependent toward dehydrogenation of formic acid, while $Co_9Ag_{21}Pd_{70}$@-MIL-101 exhibits exceedingly high catalytic activity, with the turnover frequency value of 98 h^{-1}, and 100 % hydrogen selectivity at 50 °C.

Graphical Abstract Highly dispersed ternary CoAgPd NPs have been successfully immobilized on the pores of MIL-101 by using a simple liquid impregnation method for the first time. The resultant catalysts are composition dependent toward dehydrogenation of formic acid, while $Co_9Ag_{21}Pd_{70}$@MIL-101 exhibits exceedingly high catalytic activity, with TOF value of 98 h^{-1}, and 100 % hydrogen selectivity at 50 °C

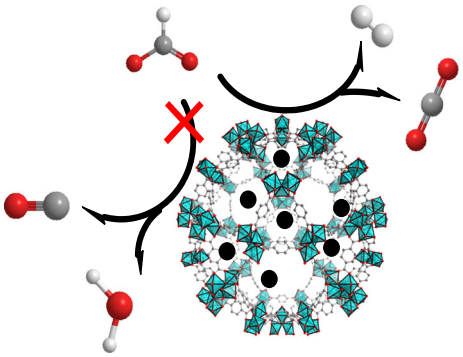

Keywords Hydrogen storage · MIL-101 · Formic acid

1 Introduction

In recent years, due to the high specific surface area and tunable pore size, porous metal-organic frameworks (MOFs) have attracted growing attention in the application of gas sorption and storage [1, 2], molecular recognition and separation [3, 4], drug delivery [5] catalysis [6, 7] and et al. Given the similarity to zeolites, loading metal nanoparticles (NPs) into the pores of MOFs is expected to control the limited growth of metal NPs in the confined cavities, and produce monodisperse NPs, which could further increase their catalytic activities [8, 9]. However, up to now, reports about MOFs supported metal NPs are mainly focused on unitary and binary systems while the ternary metal NPs supported on MOFs with more obvious synergistic effect, to the best of our knowledge, has not been reported yet.

Electronic supplementary material The online version of this article (doi:10.1007/s10562-015-1671-8) contains supplementary material, which is available to authorized users.

✉ Kai Hu
kaihu@whu.edu.cn

[1] College of Chemistry and Molecular Sciences, Wuhan University, Wuhan, Hubei 430072, People's Republic of China

[2] Suzhou Institute of Wuhan University, Suzhou, Jiangsu 215123, People's Republic of China

On the other hand, the safe and efficient storage of hydrogen is essential for the development of a hydrogen-based energy infrastructure. For the last few decades, many carriers were proposed for suitable hydrogen storage, including metal hydrides [10], sorbent materials [11], and chemical hydrides [12, 13].Notably, formic acid (FA), a major product of biomass processing, has attracted considerable attention as a safe and convenient hydrogen storage material due to its high hydrogen content, non-toxicity, liquid at room temperature and easy recharging ability [14]. Hydrogen stored in FA can be released through a catalytic dehydrogenation way (Eq. 1). However, carbon monoxide (CO), which is fatal poison to catalysts, generated from the undesirable dehydrogenation way (Eq. 2) should be avoided [15]. Recently, much progress in selective dehydrogenation of FA at remarkable hydrogen generation rates has been made [16, 17]. Among them, Pd based noble metal nanocatalysts have attracted much attentions due to their high catalytic performances. However, the unitary Pd NPs are prone to deactivation throughout the adsorption of CO intermediate. Therefore, many efforts have been developed to increase the CO resistance and catalytic performance of Pd NPs by alloying or forming core–shell structure [18–21]. However, large-scale commercialization is still restricted mainly by their high costs and low reserves in the earth's crust. Therefore, it is highly desirable to reduce or replace Pd based catalysts by integration of low-cost metals and further increase their CO resistance and catalytic activity [17, 22–25].

$$\begin{aligned} &HCOOH\,(1) \;\rightarrow\; H_2\,(g) + CO_2\,(g) \\ &\Delta G_{298K} \;=\; -35.0\,KJ\,mol^{-1} \end{aligned} \tag{1}$$

$$\begin{aligned} &HCOOH\,(1) \;\rightarrow\; H_2O\,(1) + CO\,(g) \\ &\Delta G_{298\,K} \;=\; -14.9\,KJ\,mol^{-1} \end{aligned} \tag{2}$$

Herein, for the first time, ternary CoAgPd NPs have been successfully immobilized on the pores of MIL-101 by using a simple impregnation method. Non-noble metal Co as introduced to form alloy with noble metal Ag and Pd. It is reported that Co can prevent the primary AgPd NPs from aggregation [19]. MIL-101, a chromium-based MOF, $Cr_3F(H_2O)_2O[(O_2C)C_6H_4(CO_2)]_3 \cdot nH_2O$ (n = 25), is an excellent MOF as the support material because of its extra high specific surface area, its pore volume, and its high thermal stability (up to 300 °C) and high stability in water. It has two hydrophilic mesoporous cavities (2.9 and 3.4 nm) accessible through two microporous windows of about 1.2 and 1.6 nm in diameter, respectively [26, 27],which can confined the growth of NPs in the framework. Formate ion, as a conjugate base of formic acid, is usually added to as a catalyst promoter for FA dehydrogenation [28–30]. The formate additive is believed to introduced a favourable adsorption configuration of FA to accelerate the kinetics of FA decomposition [30, 31] and/or to act as an active intermediate [32, 33] to facilitate CO productions. In this work, the ternary NPs catalysts was used for the dehydrogenation of HCOOH + HCOONa in solution. As expected, compared to their unitary and binary counterparts as well as ternary CoAgPd NPs on other commercial supported materials, the resultant $Co_9Ag_{21}Pd_{70}$@MIL-101 NPs exert superior catalytic activity and 100 % hydrogen selectivity toward dehydrogenation of FA under mild conditions.

2 Experimental

2.1 Chemicals and Materials

All chemicals were commercial and used without further purification. Chromic nitrate nonahydrate ($Cr(NO_3)_3{\cdot}9H_2O$, Sinopharm Chemical Reagent Co., Ltd., 99 %), Cobalt chloride hexahydrate ($CoCl_2{\cdot}6H_2O$, Sinopharm Chemical Reagent Co., Ltd, ≥99 %), Silver nitrate ($AgNO_3$, AR), Palladium chloride ($PdCl_2$, Great Wall Reagent Co., Ltd., 99 %), nickel chloride hexahydrate ($NiCl_2{\cdot}6H_2O$, Sinopharm Chemical Reagent Co., Ltd., ≥99 %), copper chloride dihydrate ($CuCl_2{\cdot}2H_2O$, Sinopharm Chemical Reagent Co., Ltd., ≥99 %), iron chloride tetrahydrate ($FeCl_2{\cdot}4H_2O$, Sinopharm Chemical Reagent Co., Ltd., ≥99 %), Sodium borohydride ($NaBH_4$, Sinopharm Chemical Reagent Co., Ltd., 96 %), Sodium formate ($HCOONa{\cdot}2H_2O$, Sinopharm Chemical Reagent Co., Ltd., 99 %), FA (HCOOH, Sigma-Aldrich, 98 %), Terephthalic acid ($HO_2CC_6H_4CO_2H$, Sinopharm Chemical Reagent Co., Ltd., 99 %), Acetic acid (CH_3COOH, AR, Sinopharm Chemical Reagent Co., Ltd.), Ethanol (C_2H_5OH, Sinopharm Chemical Reagent Co., Ltd., >99.8 %) were used as received. We use ordinary distilled water as the reaction solvent.

2.2 Synthesis of MIL-101

MIL-101 was synthesized using the reported procedure [34]. Terephthalic acid (332 mg, 2.0 mmol), $Cr(NO_3)_3{\cdot}9H_2O$ (800 mg, 2.0 mmol), CH_3COOH (1.5 mL) and deionized water (10 mL) were placed in a 50 mL Teflon-liner autoclave and heated at 200 °C for 8 h. After natural cooling, the suspension was centrifuged to separate the green powder of MIL-101 with formula $Cr_3F(H_2O)_2O[(O_2C)C_6H_4(CO_2)]_3{\cdot}nH_2O$ ($n \leq 25$), and then further dispersed in ethanol under sonication. The mixture was centrifuged to collect green solid and finally dried overnight at 150 °C under vacuum for further use.

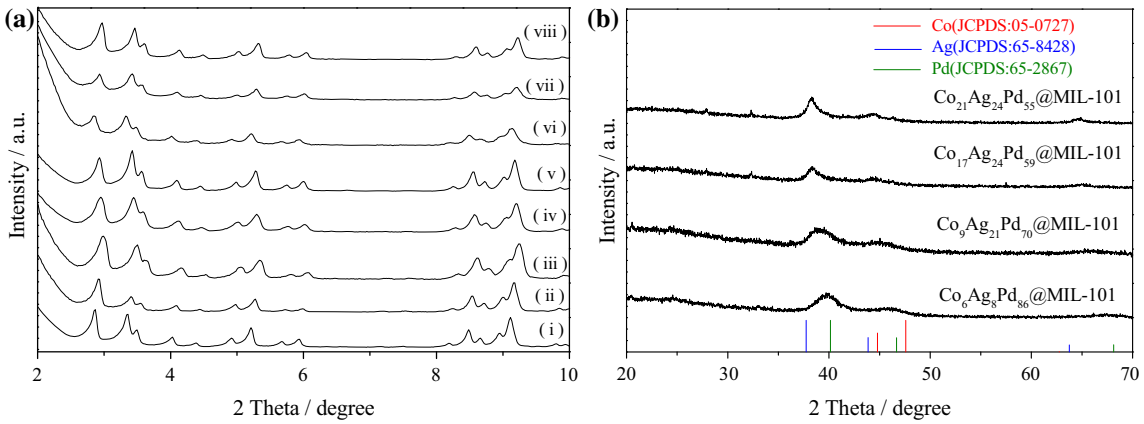

Fig. 1 **a** The low-angle Powder X-ray diffraction patterns of s (*i*) $Co_6Ag_8Pd_{86}$@MIL-101, (*ii*) $Co_9Ag_{21}Pd_{70}$@MIL-101, (*iii*) $Co_{17}Ag_{24}Pd_{59}$@MIL-101, (*iv*) $Co_{21}Ag_{24}Pd_{55}$@MIL-101, (*v*) $Co_{33}Ag_{15}Pd_{52}$@MIL-101, (*vi*) $Co_{54}Ag_{13}Pd_{19}$@MIL-101, (*vii*) $Co_{68}Ag_8Pd_{86}$@MIL-101 and (*viii*) $Co_{89}Ag_7Pd_4$@MIL-101. **b** The wide-angle PXRD of $Co_6Ag_8Pd_{86}$@MIL-101, $Co_9Ag_{21}Pd_{70}$@MIL-101, $Co_{17}Ag_{24}Pd_{59}$@MIL-101 and $Co_{21}Ag_{24}Pd_{55}$@MIL-101

2.3 Synthesis of H_2PdCl_4

A solution of tetrachloropalladinic acid (0.05 M, H_2PdCl_4) was prepared by mixing 222.5 mg of $PdCl_2$ into 25 mL of HCl (0.02 M) aqueous solution under stirring at room temperature until complete dissolution.

2.4 Synthesis of CoAgPd@MIL-101

Activated MIL-101 (100 mg) was mixed with 10 mL deionized water containing 0.2 mmol metal salts ($CoCl_2$, $AgNO_3$ and H_2PdCl_4) and stirring was continued for 8 h at 25 °C. After the impregnation, the suspension was concentrated under vacuum. The resulting mixture was then reduced by sodium borohydride ($NaBH_4$, 37.8 mg) with vigorous stirring at 25 °C to yield CoAgPd@MIL-101. For comparison, CoAgPd loaded on C, PVP, graphene and SBA-15 were prepared with the similar method.

2.5 H_2 Generation from Formic Acid Aqueous Solution

Typically, 2.0 mL aqueous solution containing the as-prepared CoAgPd@MIL-101 (100 mg) was kept in a two-necked round-bottom flask. One neck was connected to a gas burette, and the other was connected to a pressure-equalization funnel to introduce the mixed solution of formic acid (FA, 140 mg, 3 mmol) and sodium formate (SF, 70 mg, 0.67 mmol). The catalytic reaction was begun once the FA/FS solution was added into the flask with magnetic stirring. The evolution of gas was monitored by the gas burette. The reaction was carried out at 298 K under ambient atmosphere.

2.6 Recyclability Test

For recycle stability test, catalytic reactions were repeated 3 times by adding another equivalent of FA (3 mmol) and SF (0.67 mmol) into the mixture after the previous cycle.

2.7 Characterization

The as-synthesized CoAgPd@MIL-101 catalysts with different metal ratios were obtained after centrifugation, and washed with water several times before characterization. The morphologies and sizes of the samples were observed by using a Tecnai G20 U-Twin transmission electron microscope (TEM) equipped with an energy dispersive X-ray detector (EDX) at an acceleration voltage of 200 kV. Powder X-ray diffraction (XRD) patterns were measured by a Bruker D8-Advance X-ray diffractometer using Cu Ka radiation source ($\lambda = 0.154178$ nm) with a velocity of 1 min^{-1}. X-ray photoelectron spectroscopy (XPS) measurement was performed with a Kratos XSAM 800 spectrophotometer. The surface area measurements were performed with N_2 adsorption/desorption isotherms at liquid nitrogen temperature (77 K) after dehydration under vacuum at 373 K for 12 h using Quantachrome NOVA 4200e. The inductively coupled plasma-atomic emission spectroscopy (ICP-AES) was performed on IRIS Intrepid II XSP (Thermo Fisher Scientific, USA). Detailed analyses for CO_2, H_2 and CO were performed on GC-9790 (Zhejiang Fuli Analytical Instrument CO., LTD) with thermal conductivity detector (TCD) flame ionization detector (FID)-Methanator (detection limit: ~10 ppm).

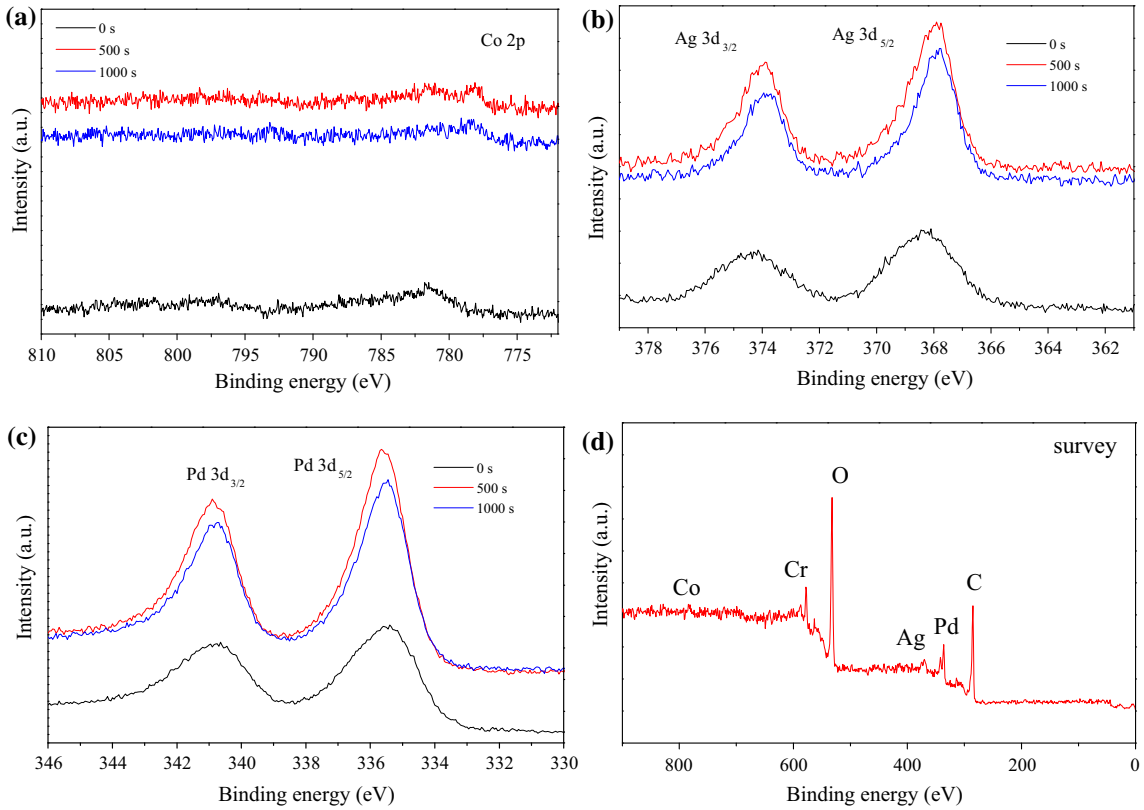

Fig. 2 The XPS spectra of **a** Co, **b** Ag and **c** Pd in CoAgPd@MIL-101 before (0 s) and after (500 and 1000 s) argon sputtering and the survey scan (**d**)

3 Results and Discussion

3.1 Structure Characters of Catalyst

CoAgPd@MIL-101 heterogeneous catalyst for dehydrogenation of FA as was prepared. There are no apparent loss of crystallinity from the low-angle powder X-ray diffraction (PXRD) patterns of all CoAgPd@MIL-101 samples compared with parent MIL-101(Fig. 1a), suggesting that the integrity of the MIL-101 framework was maintained. In addition, from the wide-angle PXRD (Fig. 1b), the diffraction peaks of CoAgPd@MIL-101 are located between the fcc diffraction peaks of Ag and Pd. Moreover, the peaks are shifted to lower angles as the content of Ag increased. These results indicate that CoAgPd is formed as an alloy structure in metal state. Furthermore, the composition of CoAgPd@MIL-101 was analyzed by inductively coupled plasma-atomic emission spectroscopy (ICP-AES) (Table S1).

The X-ray photoelectron spectroscopy (XPS) of CoAgPd@MIL-101 (Fig. 2) showed the binding energies for Pd 3d and Co 2p in CoAgPd@MIL-101 are both shifted to the higher values by about 0.6 and 1.2 eV, respectively. Whereas, Ag 3d peak for CoAgPd@MIL-101 is shifted to lower binding energies, which could be further indicative of the formation of CoAgPd alloy [22]. The formation of oxidized Co after Ar sputtering shows the alloy NPs most likely occurs during the sample preparation process for the XPS measurements [35]. Surface area of CoAgPd@MIL-101 was calculated from the N_2 isotherm using BET model

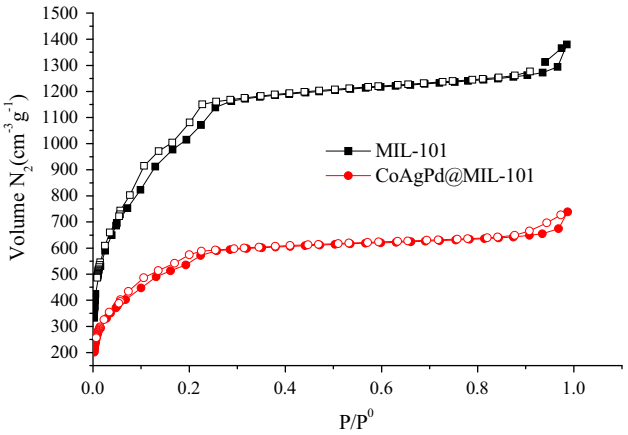

Fig. 3 N_2 sorption isotherms of activated MIL-101 and CoAgPd@-MIL-101 at 77 K. Filled and open symbols represent adsorption and desorption branches, respectively

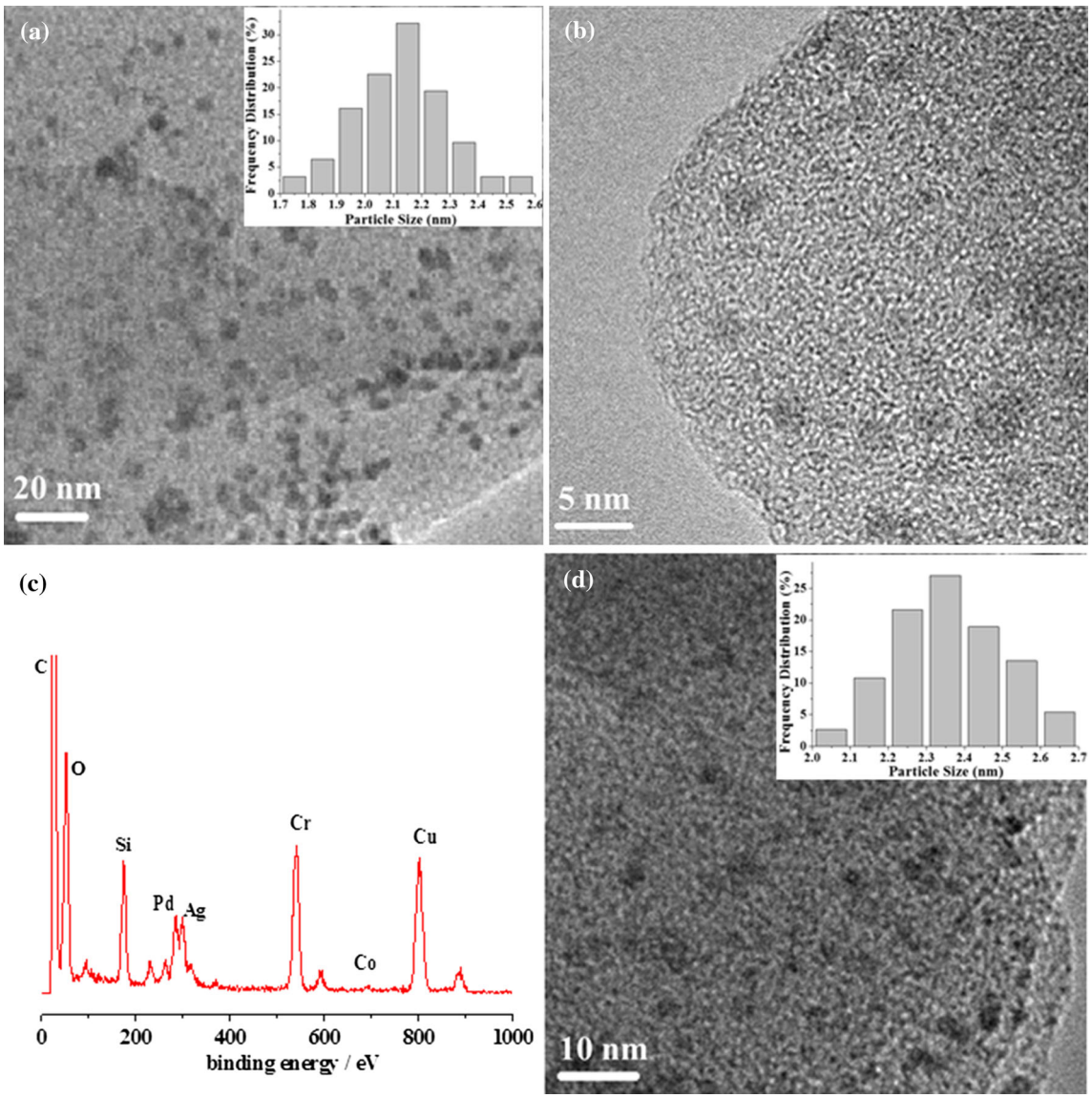

Fig. 4 **a**, **b** TEM images of CoAgPd@MIL-101with different magnifications, (**a** *inset*) Particle size distributions of CoAgPd NPs, **c** EDX of CoAgPd@MIL-101, **d** TEM images of CoAgPd@MIL-101 after three cycles

(Fig. 3). In comparison with that of MIL-101, the significant decrease in the amount of N_2 adsorption and the pore volume (Table S2) of CoAgPd@MIL-101 indicate that that the cavities of the host framework are either occupied by the dispersed CoAgPd NPs or blocked by the CoAgPd NPs [36].

The morphologies of MIL-101 immobilized CoAgPd NPs were further characterized by TEM and energy-dispersive EDX measurements (Fig. 4). The well dispersed CoAgPd NPs were successfully immobilized on the pores of MIL-101, with an average diameter of 2.1 ± 0.4 nm, which indicated that that ternary CoAgPd NPs were small enough to be encapsulated into the two mesoporous cavities of MIL-101 (2.9 and 3.4 nm), and big enough to be confined in the pores of the framework by the windows of MIL-101 (1.2 and 1.6 nm) [27]. The EDX spectrum (Fig. 4c) further confirms the presence of CoAgPd.

3.2 Catalytic Performance

The catalytic activities of ternary CoAgPd@MIL-101 with different compositions and their binary, unitary counterparts for hydrogen generation from FA have been performed over all the samples at 50 °C in the presence of sodium formate (HCOONa, SF) as shown in Fig. 5a. Their catalytic activities were strongly depended on the composition of CoAgPd NPs. Obviously, $Co_9Ag_{21}Pd_{70}$@MIL-101 exhibits highest catalytic activity with the turnover

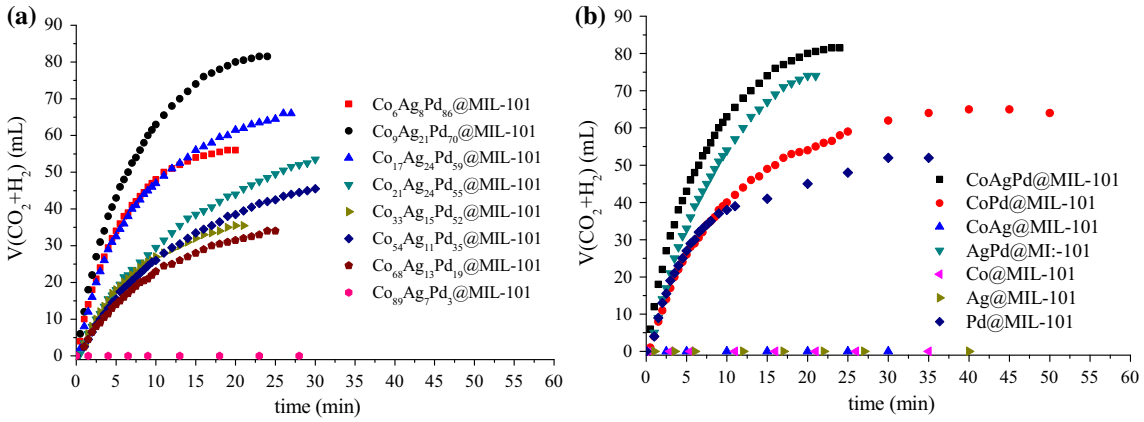

Fig. 5 Gas generation by decomposition of FA/SF with **a** composition of CoAgPd supported on MIL-101 and **b** monometallic and bimetallic countparts versus time at at 50 °C. (catalyst = 100 mg, FA = 140 mg, SF = 70 mg)

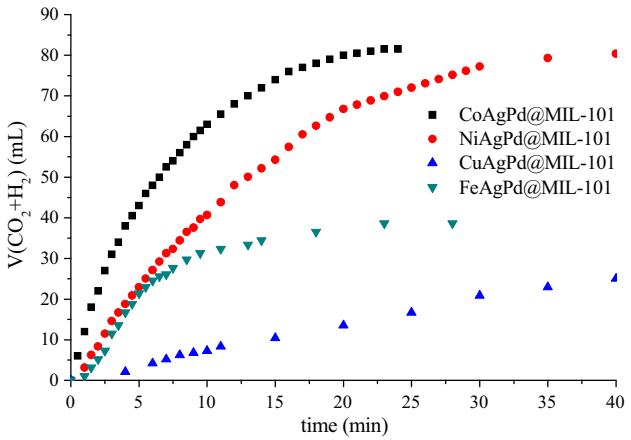

Fig. 6 Gas generation by decomposition of FA/SF with CoAgPd@MIL-101, NiAgPd@MIL-101, CuAgPd@MIL-101 and FeAgPd@MIL-101. (catalyst = 100 mg, FA = 140 mg, SF = 70 mg)

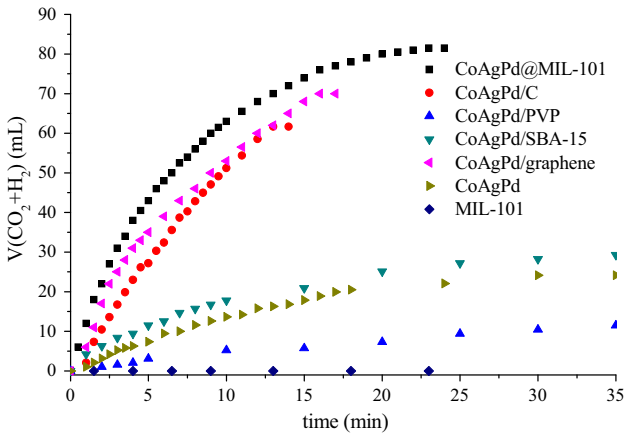

Fig. 7 Gas generation by decomposition of FA/SF with MIL-101 and CoAgPd NPs loaded on different supports. (catalyst = 100 mg, FA = 140 mg, SF = 70 mg)

frequency (TOF) value of 98 h^{-1} at 50 °C among all the catalysts tested, this value is higher than most of the reported values (Table S3). To further studied the effect of temperature on dehydrogenation of FA catalyzed by $Co_9Ag_{21}Pd70$@MIL-101 catalyst, the dehydrogenation reactions were carried out at temperatures ranging from 50 to 80 °C. The Arrhenius plot of ln *k* vs. 1/T for the catalyst is plotted Fig. S1, from which the apparent activation energy (Ea)was determined to be approximately 24.21 kJ mol^{-1}, which is lower than most of reported values (Table S3). By gas chromatography, CO-free mixture of H_2 and CO_2 were detected (Fig. S2), indicating the excellent H_2 selectivity for FA dehydrogenation by the as-synthesized CoAgPd@MIL-101.

From Fig. 5b, it is clear that Pd is crucial active metal in all catalysts. Without Pd addition, catalysts as Ag@MIL-101, Co@MIL-101 and CoAg@MIL101 show no activity. Furthermore, it is found that the co-incorporation of Co and Ag into the Pd structure to form CoAgPd alloy structure significantly enhanced the catalytic activity. For comparison, NiAgPd@MIL-101, CuAgPd@MIL-101 and FeAgPd@MIL-101 were synthesized using the similar method, their catalytic performances were all inferior to that of CoAgPd@MIL-101, further indicating the synergistic effect of Co in the ternary CoAgPd@MIL-101 catalyst (Fig. 6).

Furthermore, to study the effects of different supported materials on the catalytic activity, ternary CoAgPd NPs supported on different materials such as carbon black, PVP, graphene, and SBA-15 were synthesized and their catalytic performances were tested. As shown in Fig. 7, the catalytic performances of all the catalysts tested were all inferior to that of CoAgPd immobilized on MIL-101. In addition, the CoAgPd NPs without supported materials and MIL-101 are both inactive. These results highlight the key fact of MIL-

101 in promoting the catalytic activity and the synergistic effect of ternary CoAgPd NPs and MIL-101.

The ratio of sodium formate/formic acid (FA/SF) has a great effect on the catalytic activity of nanocatalysts. FA/SF solutions with different FA/SF mass ratios were studied over $Co_9Ag_{21}Pd_{70}$@MIL-101 at 50 °C. We can see from Fig. S3 that no gas can be generated over the as-synthesized catalyst from SF without FA and highest catalytic activity exhibited when the mass ratio of FA/SF is 2:1.

The stability test of $Co_9Ag_{21}Pd_{70}$@MIL-101 catalyst showed that there is slight decrease in catalytic activity and no change in the hydrogen selectivity after the third run (Fig. S4). The TEM of CoAgPd@MIL-101 catalyst after three cycles shown that the CoAgPd NPs were well dispersed on the MIL-101 without no obvious agglomeration (Fig. 4d). However, the particle size was increased, which may be the reason for the decrease in their catalytic activity. Further work on the enhancement of the stability of the as-synthesized catalysts is still underway.

4 Conclusion

In summary, we have developed a highly efficient heterogeneous catalyst CoAgPd@MIL-101 in dehydrogenation of FA for chemical hydrogen storage. It exhibits a marked superiority over the unitary and binary or ternary counterparts with other compositions, indicating a strong molecular-scale synergy of CoAgPd alloy. In addition, compare with CoAgPd NPs supported on other supported materials, the CoAgPd NPs immobilized on the pores of MIL-101 exhibit highest catalytic performances, highlighting the crucial roles of MIL-101. The combination of high activity (TOF: 98 h^{-1}, 50 °C) and 100 % selectivity, as well as integration of low-cost metal may promote the practical application of FA for chemical hydrogen storage in the fuel-cell hydrogen economy. Furthermore, this simple impregnation method could open up a new avenue for preparing other multiple metal NPs confined inside the pores of MOFs for more applications.

Acknowledgments This work was financially supported by the National Natural Science Foundation of China (21201134, 21571145), the Natural Science Foundation of Jiangsu Province (BK20130370) and Large-scale Instrument and Equipment Sharing Foundation of Wuhan University.

References

1. Yang QY, Liu DH, Zhong CL, Li JR (2013) Chem Rev 113:8261
2. Furukawa H, Cordova KE, O'Keeffe M, Yaghi OM (2013) Science 341:974
3. Bloch WM, Babarao R, Hill MR, Doonan CJ, Sumby CJ (2013) J Am Chem Soc 135:10441
4. Bradshaw D, Garai A, Huo J (2012) Chem Soc Rev 41:2344
5. Wang C, Liu DM, Lin WB (2013) J Am Chem Soc 135:13222
6. Aijaz A, Akita T, Tsumori N, Xu Q (2013) J Am Chem Soc 135:16356
7. Hosseinzadeh R, Aghili N, Tajbakhsh M (2015) Catal Lett. doi:10.1007/s10562-015-1622-4
8. Moon HR, Limb DW, Suh MP (2013) Chem Soc Rev 42:1807
9. Kuo CH, Tang Y, Chou LY, Sneed BT, Brodsky CN, Zhao Z, Tsung CK (2012) J Am Chem Soc 134:14345
10. Javadian P, Sheppard DA, buckley CE, Jensen TR (2015) Nano Energy 11:96
11. Suh MP, Park HJ, Prasad TK, Lim DW (2012) Chem Rev 112:782
12. Luo W, Campbell PG, Zakharov LN, Liu SY (2011) J Am Chem Soc 133:19326
13. Zhou SD, Qian C, Chen XZ (2011) Catal Lett 141:726
14. Yadav M, Xu Q (2012) Energy Environ Sci 5:9698
15. Zhang ZY, Cao SW, Liao YS, Xue C (2015) Appl Catal B Environ 162:204
16. Grasemann M, Laurenczy G (2012) Energy Environ Sci 5:8171
17. Bulut A, Yurderi M, Karatas Y, Say Z, Kivrak H, Kaya M, Gulcan M, Ozensoy E, Zahmakiran M (2015) ACS Catal 5(10):6099
18. Yang L, Hua X, Su J, Luo W, Chen SL, Cheng GZ (2015) Appl Catal B Environ 168:423
19. Dai HM, Cao N, Yang L, Su J, Luo W, Cheng GZ (2014) J Mater Chem A 2:11060
20. Chen Y, Zhu QL, Tsumori N, Xu Q (2015) J Am Chem Soc 137:106
21. Yu WY, Mullen GM, Flaherty DW, Mullins CB (2014) J Am Chem Soc 136:11070
22. Hu C, Ting SW, Tsui J, Chan KY (2012) Int J Hydrog Energy 37:6372
23. Qin YL, Wang J, Meng FZ, Wang LM, Zhang XB (2013) Chem Commun 49:10028
24. Wang ZL, Ping Y, Yan YM, Wang HL, Jiang Q (2014) Int J Hydrog Energy 39:4850
25. Koós Á, Solymosi F (2010) Cata Lett 138:23
26. Gu XJ, Lu ZH, Jiang HL, Akita T, Xu Q (2011) J Am Chem Soc 133:11822
27. Férey G, Mellot-Draznieks C, Serre C, Millange F, Dutour J, Surblé S, Margiolaki I (2005) Science 309:2040
28. Fellay C, Dyson PJ, Laurenczy G (2008) Angew Chem Int Ed 47:3966
29. Zhu QL, Tsumori N, Xu Q (2015) J Am Chem Soc 137:11734
30. Jiang K, Xu K, Zou SZ, Cai WB (2014) J Am Chem Soc 136:4861
31. Wang HF, Liu ZP (2009) J Phys Chem C 113:17502
32. Joo J, Uchida T, Cuesta A, Koper MTM, Osawa M (2013) J Am Chem Soc 135:9991
33. Gao W, Keith JA, Anton J, Jacob T (2010) J Am Chem Soc 132:18377
34. Huang CY, Song M, Gu ZY, Wang HF, Yan XP (2011) Environ Sci Technol 45:4490
35. Bulut A, Yurderi M, Karatas Y, Zahmakiran M, Kivrak H, Gulcan M, Kaya M (2015) Appl Catal B Environ 164:324
36. Cao N, Su J, Wu XJ, Luo W, Cheng GZ (2014) Int J Hydrog Energy 39:9726